Marine propeller optimisation through user interaction and machine learning for advanced blade design scenarios

(article starts on next page)

Marine propeller optimisation through user interaction and machine learning for advanced blade design scenarios

Ioli Gypa, Marcus Jansson & Rickard Bensow

Published online: 11 Oct 2023.

Submit your article to this journal ↗

Article views: 154

View related articles ↗

View Crossmark data ↗

Taylor & Francis
Taylor & Francis Group

Marine propeller optimisation through user interaction and machine learning for advanced blade design scenarios

Ioli Gypa[a], Marcus Jansson[b] and Rickard Bensow[a]

[a]Mechanics and Maritime Sciences, Chalmers University of Technology, Gothenburg, Sweden; [b]Kongsberg Maritime Sweden AB, Kristinehamn, Sweden

ABSTRACT

The complexity of the marine propeller design process is well recognised and is related to contradicting requirements of the stakeholders, complex physical phenomena, and fast analysis tools, where the latter are preferred due to the strict time limitations under which the entire process is carried out. With all this in mind, an optimisation methodology has been proposed and presented earlier that combines user interactivity with machine learning and proved to be useful for a simple blade design scenario. More specifically, the blade designer manually evaluates the cavitation of the designs during the optimisation and this information is systematically returned into the optimisation algorithm, a process called interactive optimisation. As part of the optimisation, a machine learning pipeline has been implemented in this study, which is used for cavitation evaluation prediction in order to solve the user fatigue problem that is connected to interactive optimisation processes. The proposed methodology is investigated for two case studies of advanced design scenarios, relevant for a real commercial situation, that regard controllable-pitch propellers for ROPAX vessels, and the aim is to obtain a set of optimal, competent blade designs. Both cases represent scenarios with several design variables, objectives and constraints and with conditions that have either suction side or pressure side cavitation. The results show that the proposed methodology can be used as a support tool for the blade designers to, under strict time constraints, find a suitable set of propeller designs, some of which can be considered equal or even superior to the delivered design.

1. Introduction

Marine propeller design, when performed as an everyday task for industrial applications, must be carried out within strict time limitations. It is not efficient to systematically implement experiments and high-fidelity simulations in the design process, therefore fast analysis tools of lower fidelity are preferred, based on for example lifting line theory, vortex lattice and boundary element methods (BEM). Automated optimisation is increasingly investigated as a potential support tool in constrained, multi-objective problems within marine propeller design. The general concept of automated optimisation is that the most decisive design features, in terms of system performance, are parameterised and by alternating values of those design parameters, new optimal designs/solutions are created which fulfil the objectives of the problem. Depending on each propeller design and project, the design parameters are among others the propeller diameter, blade area ratio, pitch, camber, skew, rake, while the typical objectives are related to the propeller efficiency, strength, cavitation, pressure pulses and others. The overall goal through an optimisation process is to obtain one unique propeller design that is considered optimal based on the problem's objectives, constraints and requirements (Gypa 2021).

Automated optimisation is performed more systematically with the use of optimisation algorithms in order to search the design space efficiently and find one or a set of optimal designs. Population-based, nature-inspired stochastic optimisation algorithms, like genetic algorithms (GAs), particle swarm optimisation (PSO),

ant colony optimisation, are primarily utilised and preferred to for example deterministic optimisation algorithms, since they cleverly and fast guide the exploration to areas of the design space with the optimal solutions. The optimisation eventually provides the designers with a set of optimal designs (Gypa 2021).

Automated optimisation has been utilised by several research groups (Berger et al. 2014; Vesting 2015; Foeth and Lafeber 2015; Huisman and Foeth 2017; Gaggero et al. 2017; Valdenazzi et al. 2019; Törnros et al. 2019; Tadros et al. 2022; Guan et al. 2022; Karimi et al. 2022) for blade design optimisation problems. Vesting (2015) worked with automated optimisation extensively and the main focus was on the investigation of different optimisation algorithms, such as the non-dominated sorting genetic algorithm (NSGA-II) (Deb et al. 2002) and PSO, including extensions with metamodels. Different geometrical modifications and constraint-handling methods, mainly related to cavitation, were implemented in the process. Berger et al. (2014) presented an optimisation methodology for full scale propellers working behind a ship, where at a first stage a BEM tool was combined with an optimisation algorithm and at a second stage some designs were further evaluated by a Reynolds Average Navier-Stokes (RANS) tool. A similar approach was presented by Huisman and Foeth (2017), where the NSGA-II was combined with a BEM tool for solving two propeller optimisation tools with several objectives and constraints. Gaggero et al. (2017) worked on a multi-objective optimisation problem of a cavitating propeller of a high-speed craft, where a genetic algorithm (GA) was combined with a BEM tool.

After the optimisation, some designs were manually selected by the blade designer for further evaluation by a RANS-based CFD tool and one design was validated by cavitation tunnel tests. Valdenazzi et al. (2019) presented a practical optimisation tool for the hydro-acoustic optimisation of naval propellers, which was performed in three stages and in each stage different optimisation objectives and analysis tools were selected. An industrial application was presented by Törnros et al. (2019), where a competitive multi-objective PSO was combined with a BEM tool for the optimisation of a propeller geometry in a complex scenario with three operating conditions. Some Pareto designs were further evaluated by a RANS-based CFD tool. Tadros et al. (2022) coupled a commercial propeller design tool with a non-linear interior-point algorithm and utilised it for an optimisation problem with the overall goal to select two optimal ducted controllable-pitch propellers (CPPs) and with two objectives, to maximise the efficiency and minimise the fuel consumption. An automated optimisation methodology was presented by Guan et al. (2022), where fluid-structure interaction, design of experiment and the NSGA-II were combined with overall goal to ensure the desirable thrust and the structural strength of the propeller. Karimi et al. (2022) suggested an improvement on the standard PSO by modified chaotic self-governing groups of particles and applied this for the solution of a two-objective marine propeller optimisation problem. Most of the above-mentioned studies have given satisfactory results in terms of performance. However, as we have previously described in Gypa et al. (2021), automated optimisation is hard to implement in industrial applications successfully due to the following reasons:

- The optimisation algorithms are difficult to set-up to reach a converged solution; this involves the definition of the design space and the parameters that control the optimisation process.
- The different requirements on each scenario-based design situation are difficult to formulate into a single well-posed optimisation problem; e.g. several operating conditions may need to be considered, with different cavitation nuisance requirements in each.
- The constraint handling fails due to the fact that: (a) the physics involved in some constraints (e.g. erosion risk, radiated sound) is too complicated to be represented by semi-empirical evaluations within the strict time limitations, and b) the number of feasible designs developed during the optimisation can become too low to be useful.
- The performance prediction of the tools have high uncertainty in some regions and guide the optimisation in the wrong area of the design space.

Therefore it is considered more reliable and efficient to use a traditional manual design process than a fully automated optimisation (Vesting 2015; Kongsberg hydrodynamic design team 2020). Manual design is defined in this study as the design that the blade designer has designed without using any optimisation tools. The designer's expertise needs to be part of the design and optimisation procedure, rather than be replaced. Based on this, the approach we have previously followed is the interactive optimisation, where the blade designer is involved in the blade design optimisation process systematically (Gypa et al. 2020, 2021). More specifically in Gypa et al. (2021), cavitation images of the designs resulting from the optimisation were presented to the blade designer, who evaluated their cavitation characteristics and subsequently this information was utilised by the interactive genetic algorithms (IGAs) in order to guide the optimisation towards areas of the design space with high performance according to the objectives and satisfactory

cavitation characteristics according to the blade designer. The method was utilised for a simple blade design scenario with positive results.

A problem that occurs in interactive optimisation processes is that the engineers need to evaluate a high number of individuals manually, something that is laborious and leads to human fatigue (Wahde 2008). In Gypa et al. (2021), we used a machine learning (ML) classification algorithm, the support-vector machines (SVMs) (Vapnik 1995), as support in the optimisation. The designer's evaluations were used as training for the SVM model and when a new optimisation run was performed, the model gave a prediction of the cavitation evaluation of the new designs, instead of requiring manual evaluations by the designer. The ML implementation was further developed in Gypa et al. (2022), and a machine learning pipeline (MLP) was used that investigated five ML classification algorithms instead of only one, with the aim to ensure as high prediction accuracy as possible. Doijode et al. (2022a, 2022b) also approached the marine propeller optimisation problem by combining a dynamic optimisation method with supervised and unsupervised machine learning methods and a BEM analysis tool and the results showed a 30% reduction in computational cost compared to a traditional automated optimisation approach.

In the present study, the proposed methodology that combines the interactive optimisation with the MLP as an implemented part of the optimisation, is used for two case studies for advanced design scenarios with several design variables, objectives and constraints, and with conditions that have either suction side (SS) or pressure side (PS) cavitation. The overall goal is to investigate how the proposed methodology performs in a more complex scenario and if it is actually possible to obtain solutions that are competent and equivalent or even better than the manual design within limited time.

2. Methodology

The general concept of the methodology is that an optimisation process has as a starting point a baseline propeller geometry and the goal is to obtain a new optimised geometry with higher performance and with a satisfactory and feasible geometry, with satisfactory cavitation performance and characteristics, based on the designer's preference, and all this in a realistic time frame. In the proposed methodology interactive optimisation with a machine learning pipeline are combined. The entire interactive optimisation and MLP framework is presented in Figure 1 and the methodology is described in this section.

The required input for the optimisation is a baseline geometry and a well-defined optimisation set-up. The baseline is provided by the blade designer, who defines the design variables of the optimisation problem, along with the variable ranges, the objectives, the constraints and the optimisation parameters. In the tools of the proposed methodology, B-splines are utilised to represent the curves of the distributions of all design variables and this is described in detail in Gypa et al. (2023). The optimisation parameters depend on the selected optimisation algorithm and in the proposed methodology the NSGA-II is utilised. Thus the parameters are related to the size of the population, number of generations, different operators like mutation, crossover etc.

The optimisation starts by running the NSGA-II, which searches the design space in a smart manner and guides the optimisation towards areas of the design space with high performance. The goal of using the NSGA-II, or any optimisation algorithm, is to obtain a detailed Pareto frontier efficiently, that fulfils the objectives in the best way possible. Optimisation processes usually consist of
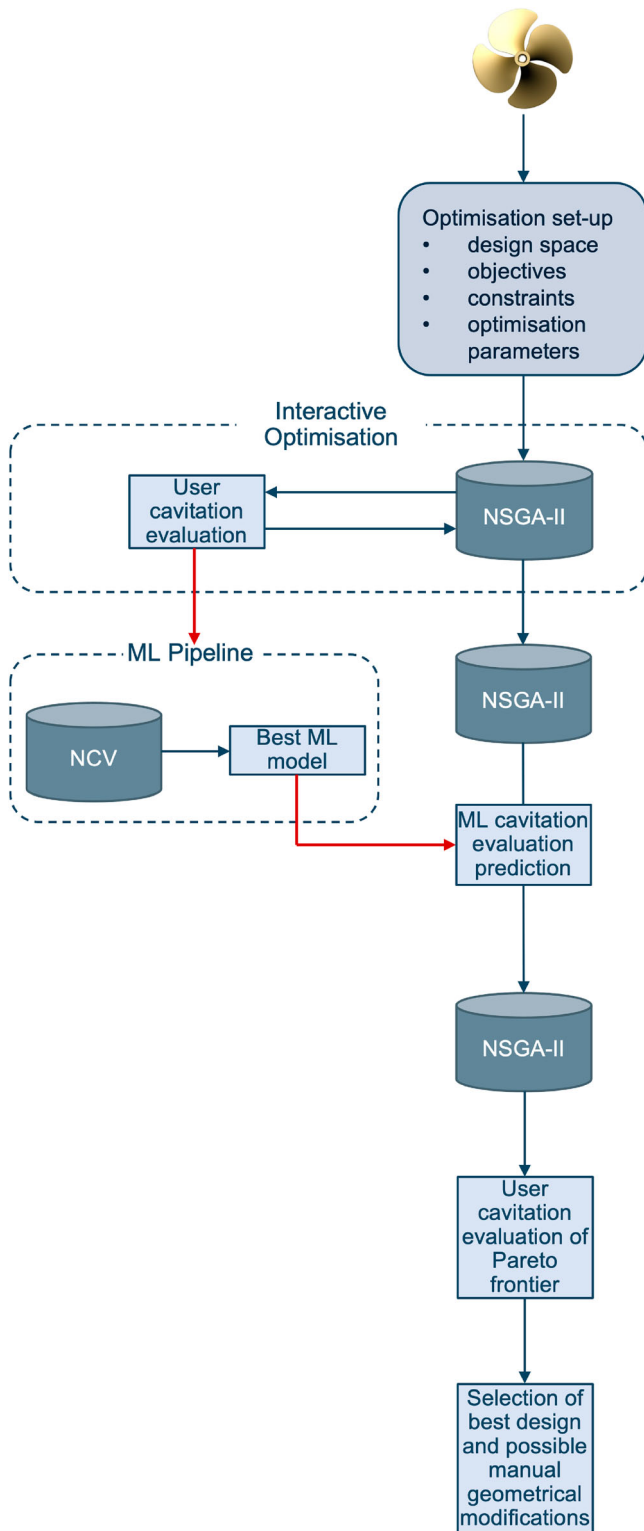
Figure 1. Interactive optimisation and MLP framework (This figure is available in colour online).

several smaller optimisation cycles, which are referred as optimisation runs, and they last from initiating them with a new set-up or input until pausing them manually or finishing the loop.

After each of the initial optimisation runs, typically of smaller size, the cavity shapes of all the designs are presented to the designer and subsequently the designer decides which designs represent geometries that result in satisfactory cavitation or not. The designs with non-satisfactory cavitation characteristics are rejected by the designer, whereas the remaining designs are considered accepted and are candidates for continuation to the next optimisation run. An example of how the cavitation images are presented to the designers during the cavitation evaluation process is shown in Figure 2. The designs are first presented to the designer, as in Figure 2(a), who rejects those designs with non-satisfactory cavity shape, depending on the demands of the project, as in Figure 2(b).

One of the key parameters of the IGAs is the number of individuals per generation, as the first generation of the next optimisation run will be comprised of only accepted designs from the previous round. If the required number of individuals for the next run is larger than the number of accepted designs, then mutation and crossover are used for the accepted individuals to create new ones in order to fill in the missing individuals; if the number is smaller, then the accepted individuals are sorted according to the NSGA-II and only the best are passed on to the next run; if the number is equal, then the first generation is comprised of all previously accepted designs.

The optimisation runs that involve manual evaluations compose the interactive optimisation process. The goal is to promote areas of the design space that suits the designer's preferences on cavitation performance, so that the algorithm goes towards those areas in the following runs. The designer decides how many interactive runs are required. By combining the NSGA-II with the manual cavitation evaluations, we aim for high performance and for feasible propeller geometries in terms of cavitation performance according to the guidance of the designer.

The next step is to use all this information produced by the interactive optimisation, in order to speed up the optimisation process by training an ML model and predicting the cavitation evaluation of the following runs. The ML model is an optional support function, proven to be useful for runs with large populations, that reduces the risk of user fatigue by performing automatic evaluations. More specifically, an MLP has been implemented in the optimisation, where the entire dataset of the interactive optimisation is used as input. Nested cross-validation (NCV) is used for investigating various hyperparameters of different ML algorithms and finally have the best model for each algorithm as an output. The best output of these models is the one that has the hyperparameters that give the highest accuracy and this is selected as the final model. This final model is used for cavitation nuisance prediction of new optimisation runs. Further information on the MLP is presented in Section 2.1.

While performing the entire process of the MLP, one or more new optimisation runs are carried out, where there is no interactivity included. These runs have a larger total population, in order to produce more designs, and the resulting ML model of the MLP is used for prediction of the cavitation evaluation. Input in this model is the dataset of the interactive optimisation, including the binary manual cavitation evaluation by the designers, which trains the model. When the model is trained, a prediction is done for the cavitation evaluation of the new dataset from the new optimisation runs.

A final run is performed and at the end of it, the designer evaluates the cavity shape only of the designs that compose the Pareto frontier. The designer decides on one or a set of the most suitable optimal designs, among the accepted ones, compares them to the baseline, selects one design and performs minor manual geometrical modifications, if necessary. This design is the trade-off between the objectives, and the quantitative and qualitative constraints.

Note that the blade designers are not involved in the ML process at all and no prior knowledge on ML is required for using the optimisation tool. The blade designers are only asked to manually
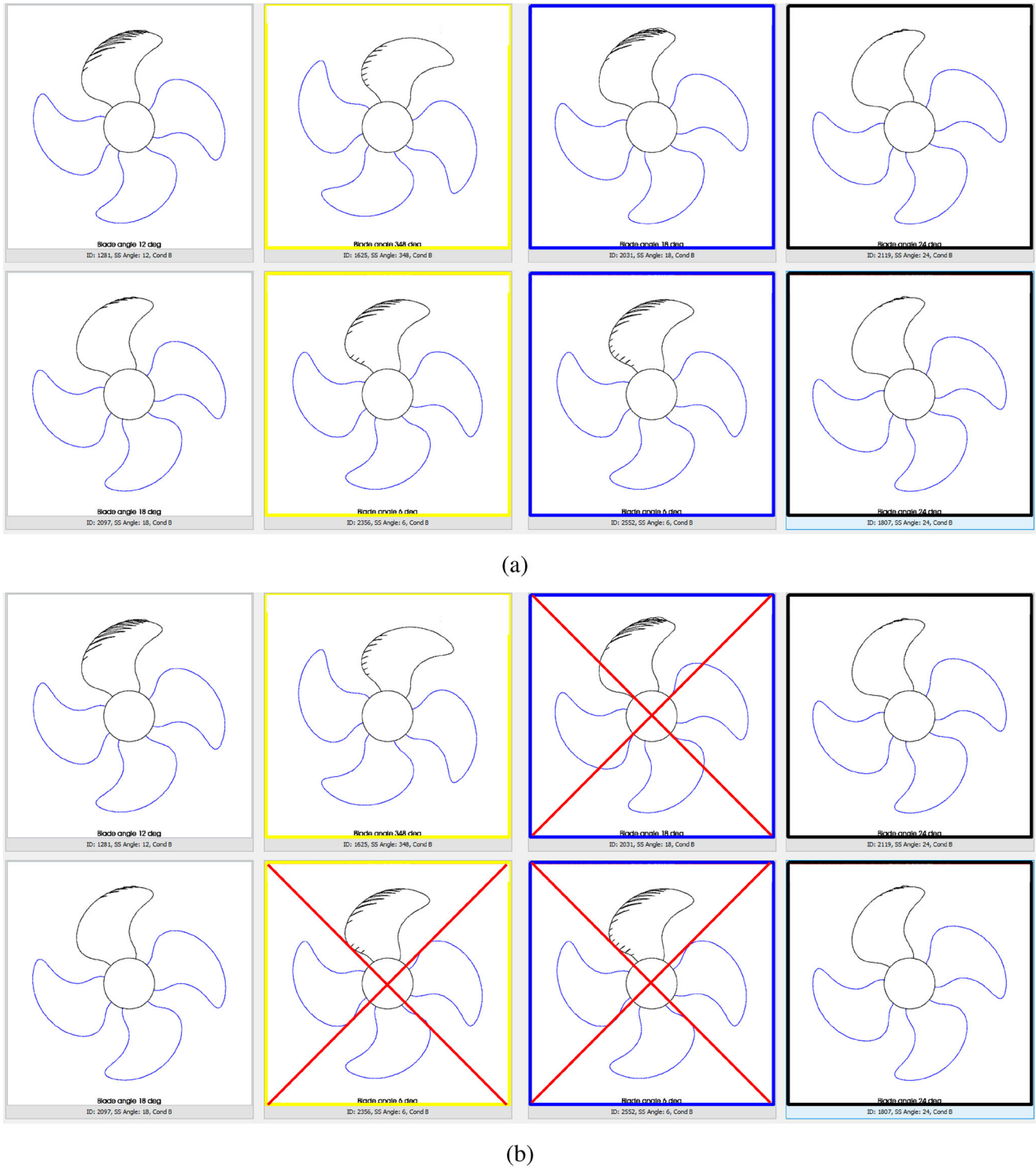
(a)

(b)

Figure 2. Cavitation evaluation dialogue box (a) Designs with cavity shape presented to the designer. (b) Rejected designs by designer (This figure is available in colour online).

evaluate cavitation characteristics at specific runs and to evaluate the final Pareto frontier, so that they decide on the final designs. The ML process gives as an output the accepted and rejected designs directly, based on the predicted cavitation evaluation.

2.1. Machine learning pipeline

The MLP has been described in detail in Gypa et al. (2022), and is summarised here for completeness. The input of the MLP involves the most important features (input features) of the dataset from the interactive optimisation and the binary manual evaluation by the blade designer. Then NCV, nested cross-validation, is used, which is an effective way to incorporate hyperparameter tuning of different ML algorithms. The NCV process has two main loops, the outer and the inner, which are shown in Figure 3. K-fold cross-validation (CV) is carried out in both loops. The purpose of the outer loop is to split the dataset into training and testing sets K_1 times, by using K-fold CV, and later input each training set
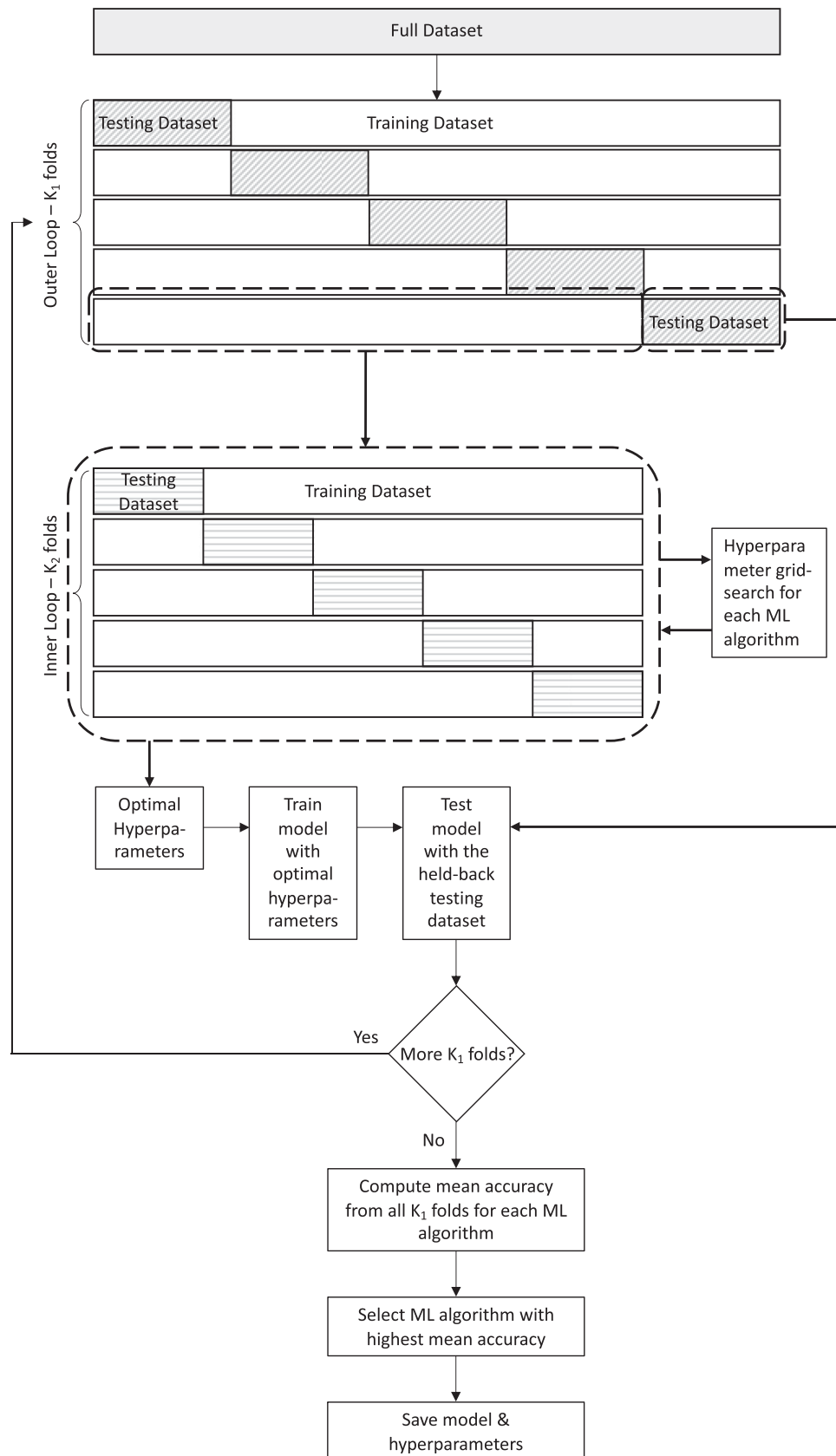
Figure 3. NCV process (This figure is available in colour online). Gypa et al. (2022)

into the inner loop. The testing sets will be used in the end for validation of the best models.

The purpose of the inner loop is to investigate which hyperparameters are the best for the targeted ML algorithm, in order to achieve the highest accuracy. This is done by first splitting the input dataset (which is the training dataset of the outer algorithm) into training and testing sets K_2 times, again by using K-fold CV. Then the values of the hyperparameters are explored through the grid search method, which is an exhaustive search process that loops through a pre-defined hyperparameter space of the targeted algorithm. Every combination of hyperparameters is fitted to the ML algorithm for each one of the K_2 training sets, and the accuracy is validated through the inner testing sets. The ML algorithm is finally refitted on the whole dataset by using the best found hyperparameters and the accuracy of the model is computed.

Due to the fact that we compare also different ML algorithms, there is one additional loop in the methodology, where the inner loop of the NCV process is repeated for each one of the algorithms. Note that each algorithm has different hyperparameters, and their ranges must be defined before the NCV process begins.

The output is one model for each ML algorithm by the inner loop, where the best hyperparameters have been selected. In the outer loop, the mean prediction accuracy is computed for each algorithm and the one that offers the highest accuracy is selected. This is considered the best model of the pipeline and is saved. When there is a new dataset, it is inputted in the best model and a prediction is done for the cavitation of the designs of the new dataset. The entire ML process has been implemented with the aid of the Scikit-learn machine learning library in Python (Pedregosa et al. 2011).

2.2. Computational tools

The hydrodynamic analysis tool we use in this study for the prediction of the propeller performance and the sheet cavitation is the vortex lattice method code MPUF-3A (He et al. 2010; He 2010), which has extensively been used and validated over many years (Fuhs 2005; Moulijn 2015). The geometry of the propeller blade is represented by a lattice of discrete vortices and sources, distributed on the mean camber surface of the blade (Vesting 2015). The kinematic boundary condition on the blade surface is considered for the strength of the vortices, where the wetted portion of the blade surface is impermeable to the fluid, and the Kutta condition is applied at the trailing edge, where the flow should leave the trailing edge in a tangential direction (Lee 1979).

The cavitation prediction is based on an iterative process, according to Kerwin et al. (1986), where a 2D cavitating profile section is considered and the cavity interface is represented by including sources whose strengths must be solved for in each time step. For the 3D solution, the cavity length is adjusted for all sections for the time step. This is done by considering radial stripes of the blade that are solved until convergence is accomplished, starting from the hub until the tip of the blade and back. Each blade section is thus constructed by this set of stripes in the flow field by combining the undisturbed inflow and the induced flow of the other stripes. The solutions are computed for only one blade, the keyblade, in order to save computational cost. Subsequently, it is assumed that the strengths of the vortices and sources on the other blades correspond to those that were calculated for the keyblade (Vesting 2015) at that position. Additionally, in this study a fixed blade wake is being taken into consideration. MPUF-3A includes also the effect of the hub, the wake alignment in circumferentially averaged inflow with an arbitrary shaft inclination angle and the nonlinear thickness loading coupling (Kinnas et al. 2003).

3. Case studies

The proposed methodology is tested by investigating two case studies with two separate propeller designs, Design I and Design II. Both designs regard twin CPPs for two ROPAX vessels, operating with constant engine rpm and represent commercially relevant tasks. The mission profile for each vessel/propeller is different, but the goal for both cases is to investigate the ability to find good blade designs that fulfil the customer requirements through the proposed optimisation procedure; the attained designs are compared with the delivered manual design by the blade designer. Both cases represent complex scenarios with several design variables, objectives and constraints, and the last are both quantitative and qualitative. In addition to this, operating conditions with cavitation on either the SS or the PS are investigated, something that further perplexes the entire process. The challenge for both designs is that except improving the performance of the objectives, when most of them are contradicting, the cavity shape should be controlled as well, based on the preference of the designer. The task of the designers prior to the optimisation is to define the most important objectives of each problem, select the design variables that affect those objectives and set-up the constraints. The selection of the design variables therefore entirely depends on the propeller optimisation problem that is being solved.

3.1. Optimisation set-up

The baseline geometry for each one of the two case studies is the result of design routines based on the vessel characteristics, the mission profiles and the selected conditions. The design variables of the optimisation process for Design I are the pitch over the propeller diameter (P/D), the camber (FM) and the leading edge modification (HM), at different blade sections. The HM refers to a design enhancement done to the leading edge of the propeller blade and is utilised as a means to change the angle of attack tolerance to mitigate PS cavitation. For Design II, there are also some additional design variables, the chord length (L) and the skew (SK), at different blade sections. More details on the design space, the objectives and constraints of the two designs follow.

3.1.1. Design I

There are seven design variables ($\vec{x}$) for Design I:

- P/D at blade sections 0.194R, 0.7R and 1.0R
- FM at 0.194R, 0.7R and 0.95R
- HM at 0.8R

The P/D and FM range $\pm 10\%$ from the values of the baseline design at all blade sections. The baseline value of HM is 0, thus the designer sets some pre-defined minimum and maximum values, based on experience. Two operating conditions are investigated, which will be referred to as C_{I-A} and C_{I-B}. Condition C_{I-A} is the design condition and in condition C_{I-B} the propeller operates at a point with delivered power of approximately 40% MCR, considered as the lowest loaded condition with two operating propellers. The objectives, which are presented in Table 1, are the maximisation of the efficiency (η) in C_{I-A} and the minimisation of the cavity volume (cav-vol) in both C_{I-A} and C_{I-B}. There is one quantitative constraint, the thrust coefficient K_T, which varies $\pm 1\%$ from the baseline K_{TB} and two qualitative constraints, the shape of the cavitation at the most critical angle at the two conditions.

Table 1. Objectives and constraints – Design I.

Objective/Constraint	Description
max $f_1(\vec{x}) = \eta_{I-A}$	Maximise efficiency in C_{I-A}
min $f_2(\vec{x}) = $ cav-vol$_{I-A}$	Minimise cavity volume in C_{I-A}
min $f_3(\vec{x}) = $ cav-vol$_{I-B}$	Minimise cavity volume in C_{I-B}
$g_1(\vec{x}) = \left| \frac{K_T}{K_{T_B}} - 1 \right| \leq 1\%$	Thrust coefficient constraint
$g_2(\vec{x})$	Qualitative constraint on cavitation in C_{I-A}
$g_3(\vec{x})$	Qualitative constraint on cavitation in C_{I-B}

Table 2. Objectives and constraints – Design II.

Objective/Constraint	Description
max $f_4(\vec{x}) = \eta_{II-A}$	Maximise efficiency in C_{II-A}
min $f_5(\vec{x}) = $ pp$_{II-A}$	Minimise pressure pulses in C_{II-A}
min $f_6(\vec{x}) = $ cav-vol$_{II-A}$	Minimise cavity volume in C_{II-A}
min $f_7(\vec{x}) = $ cav-vol$_{II-B}$	Minimise cavity volume in C_{II-B}
$g_4(\vec{x}) = \left| \frac{K_T}{K_{T_B}} - 1 \right| \leq 1\%$	Thrust coefficient constraint
$g_5(\vec{x}) = $ stress load $\leq$ pre-set value	Stress load constraint in MCR condition
$g_6(\vec{x})$	Qualitative constraint on cavitation in C_{II-A}
$g_7(\vec{x})$	Qualitative constraint on cavitation in C_{II-B}

3.1.2. Design II

Design II has the following ten design variables ($\vec{x}$):

- P/D at the blade Sections 0.197R, 0.7R and 1.0R
- FM at 0.197R, 0.7R, 0.95R
- L at 0.8R
- SK at 0.6R and 1.0R
- HM at 0.8R

The values of the P/D at all blade sections, the FM at 0.7R and 0.95R, the L and the SK at all blade sections range $\pm 10\%$ from the values of the baseline design. The baseline values for the FM at 0.197R and the HM at 0.8R are 0, so some pre-set minimum and maximum values are set by the designer, based on experience. Two operating conditions are investigated here as well, referred to as C_{II-A} and C_{II-B}. Condition C_{II-A} is the design condition and in condition C_{II-B} the propeller operates at a point with delivered power of approximately 40% MCR, considered as the lowest loaded condition with two operating propellers. The objectives, which are presented in Table 2, are the maximisation of (η), the minimisation of the pressure pulses (pp) and the minimisation of cav-vol at condition C_{II-A} and the minimisation of cav-vol at C_{II-B}.

There are two quantitative constraints in this problem. The first one is the thrust coefficient K_T, which varies $\pm 1\%$ from the baseline K_{TB}. The other constraint is related to the stress load, which should not exceed a specific set value for the MCR condition. If a design exceeds this value, a penalty (Vesting 2015) is given to it and will most probably not end up in the first front of the specific generation. There are also two qualitative constraints, the shape of the cavitation at the most critical angle for the two operating conditions.

3.1.3. Baseline and manual design

The optimisation has as a starting point the baseline design, which is a basic design used as the starting point for both the manual design and the optimisation, to ensure a fair comparison. The outcome of the optimisation will be compared to the manual design,

Table 3. Performance manual Design I – percentage change compared to baseline.

Objective	Difference [%]
max η_{I-A}	0.53
min cav-vol$_{I-A}$	1.1
min cav-vol$_{I-B}$	-43.8

Table 4. Performance manual Design II – percentage change compared to baseline.

Objective	Difference[%]
max η_{II-A}	−0.21
min pp$_{II-A}$	−22.2
min cav-vol$_{II-A}$	−33.4
min cav-vol$_{II-B}$	−3.9

which is delivered for manufacturing by the blade designer. The percentage change of the performance of the objectives for the manual design compared to the baseline design is presented in Table 3 for Design I and in Table 4 for Design II. The manual Design I has better performance in efficiency and PS cavity volume, while the SS cavity volume is worse, but by only 1%. The manual Design II offers better performance in pressure pulses and in both SS and PS cavitation, while the efficiency is lower than the efficiency of the baseline design, albeit only by 0.21%.

The cavity shape for manual and baseline designs of the propellers I and II is presented in Figure 4. One observes that the cavity shape of both propeller designs is smoother on the blade of the manual design. The key blade is represented by green colour, at the critical angle where there is maximum cavity volume. For Design I, there is SS cavitation only in condition C_{I-A} and PS cavitation on condition C_{I-B}. Similarly for Design II, there is SS cavitation on condition C_{II-A} and PS cavitation on condition C_{II-B}.

3.2. Optimisation and machine learning strategy

The same optimisation strategy has been followed for both propeller designs. Three small sequential optimisation runs are performed and at the end of every run the designer evaluates all the designs. The evaluation is based on the preference of the designer, who accepts or rejects the designs. The accepted designs are the candidates for the first generation of the next optimisation run. Each run has six generations and 52 individuals, which means in total 312 designs, out of which approximately one third to one half are unique designs. This means that the blade designer evaluates approximately 120 designs after every run.

Then a fourth run is performed for 18 generations with 52 individuals per generation, which gives a total of 936 designs with approximately 300 unique designs. During this run, the data from the first three runs are utilised as input training data for the MLP. The outcome of the MLP is one 'best' ML model that gives the highest mean accuracy, based on these input data; this model is a combination of the selected ML algorithm and the selected hyperparameters. The resulting ML model is used for the cavitation evaluation of the unique designs in this larger run. The following five ML classification algorithms are used: k-nearest neighbours (Fix and Hodges 1989), neural networks (NNs) (Hopfield 1982), decision trees (Quinlan 1986), SVMs and extreme gradient boosting (Chen and Guestrin 2016).

A final fifth optimisation run is performed, consisting of 18 generations with 52 individuals per generation. The first generation of this run consists of designs that were accepted in the cavitation evaluation, which were predicted by the ML model, and offered the highest performance. At the end of this final run, the designer manually evaluates the cavitation of only the Pareto designs and decides on one best design. This then concludes the optimisation procedure.

At the end of this procedure, the optimal design is compared with the manual, in order to understand to what degree a better design has been obtained. To judge this can be a challenging task because both the objectives and the cavitation shape have to be
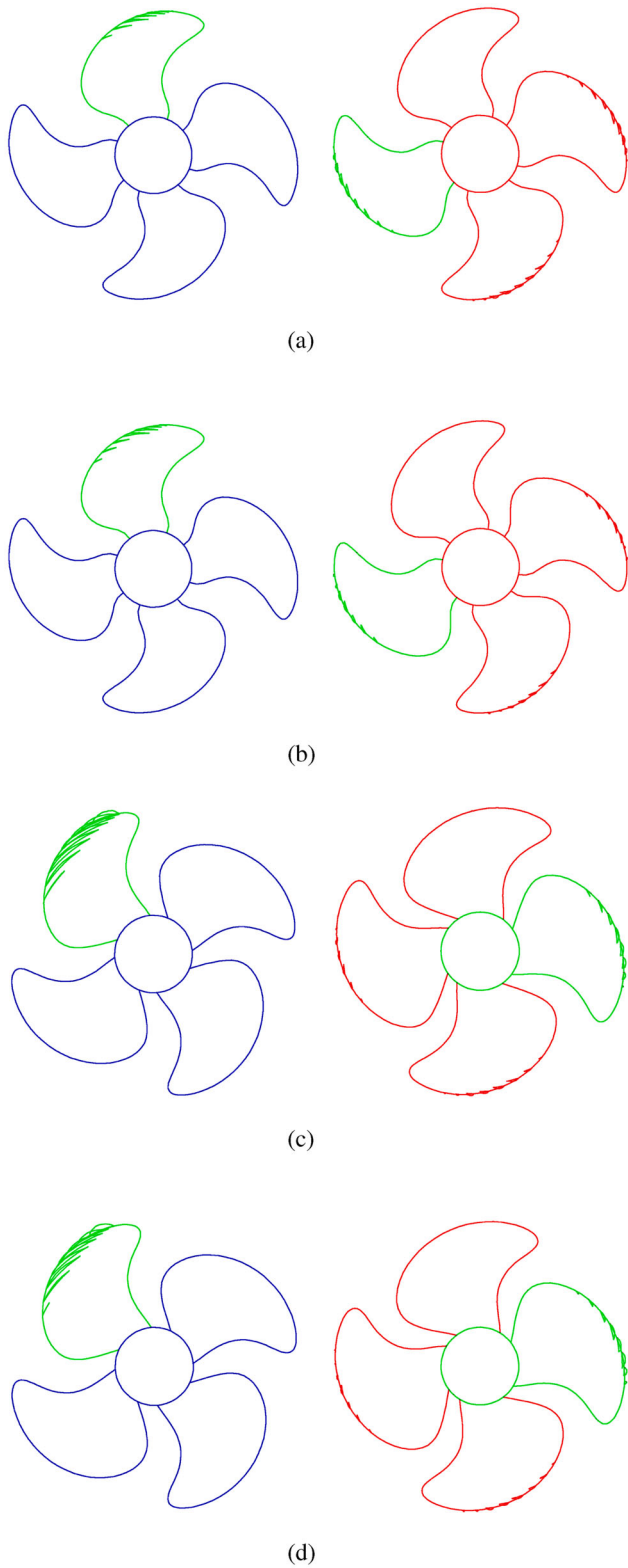
(a)

(b)

(c)

(d)

Figure 4. Cavity shape for baseline and manual designs with SS (left) and PS (right) cavitation. (a) Baseline Design I – Conditions C_{I-A} (left) and C_{I-B} (right) (b) Manual Design I – Conditions C_{I-A} (left) and C_{I-B} (right) (c) Baseline Design II – Conditions C_{II-A} (left) and C_{II-B} (right) (d) Manual Design II - Conditions C_{II-A} (left) and C_{II-B} (right) (This figure is available in colour online).

considered. In addition to this, the blade designer may perform manual geometrical modifications to the selected optimal designs, so that a feasible final geometry ready to be delivered is obtained.

4. Results

The results are presented and discussed in this section for each design separately. There are results related to the convergence of the algorithm, the final obtained Pareto frontiers, which design(s) the blade designer selected as optimal and why, which manual modifications were performed, and how the geometry of the design variables changed. There are also results related to the prediction accuracy of the ML models.

4.1. Design I

4.1.1. Convergence
In Figure 5, the convergence of the algorithm for the three objectives is presented. For each generation, designs with the best performance in each objective (maximum for efficiency, minimum for cavity volume) are plotted. The results are plotted as a percentage change to the baseline design. Since elitism is one of the main characteristics of the NSGA-II algorithm, the non-dominated designs have the highest probability of being promoted to the next generations. However, as shown in the figure, due to the user-code interaction, it seems that the non-dominated designs with the highest performance do not pass to the next generation, because they get rejected by the designer. This is shown in the three plots with the red '*' in generations 6, 12 and 18, which are the generations before performing manual evaluations. The algorithm has reached an optimum point, based on each objective, but the first generation after the manual evaluations has an optimal design with lower performance than before, but with cavitation characteristics that follow the preference of the designer. This means that the NSGA-II functions well towards finding optimum solutions, but it seems that some of those are either inefficient or undesirable. This is observed when using the MLP (generation 36) for the objective of the efficiency in Figure 5(a).

4.1.2. Pareto plots
The Pareto frontier for the performance of the three objectives is presented in three Pareto plots in Figure 6, and the results are presented as a percentage change to the baseline design. The objectives are plotted combined two by two, so that they are more comprehensible to the reader. The designer during the cavitation evaluation of the frontier has accepted 29 out of the 52 designs (56%). In Figures 6(a) and 6(b) it is shown that several non-dominated designs are better than the manual design, shown with a red '*' in the figure, when it comes to efficiency C_{I-A} vs. cavity volume C_{I-A} and efficiency C_{I-A} vs. cavity volume C_{I-B}. Regarding the objectives cavity volume C_{I-A} vs. cavity volume C_{I-B}, the manual design proved to be better than the entire Pareto front.

4.1.3. Optimal design & manual modifications
Out of the 29 accepted non-dominated designs, the designer selects one that based on their preference offers the best trade-off in terms of the objectives and the cavitation characteristics. This design, which is referred to as optimal design, is shown in all three plots of Figure 6 with the yellow circle 'o'. The designer performs some minor geometrical modifications, which are required in this project so that the geometry is ready to be delivered for manufacturing. The modifications are described below:

- Pitch curve: Local decrease at the tip and at the root up to 0.5R.
- Camber curve: Decrease at the tip due to bad shape of the profiles. Increase at 0.5 –0.8R and reduce at the root to compensate for higher pitch.
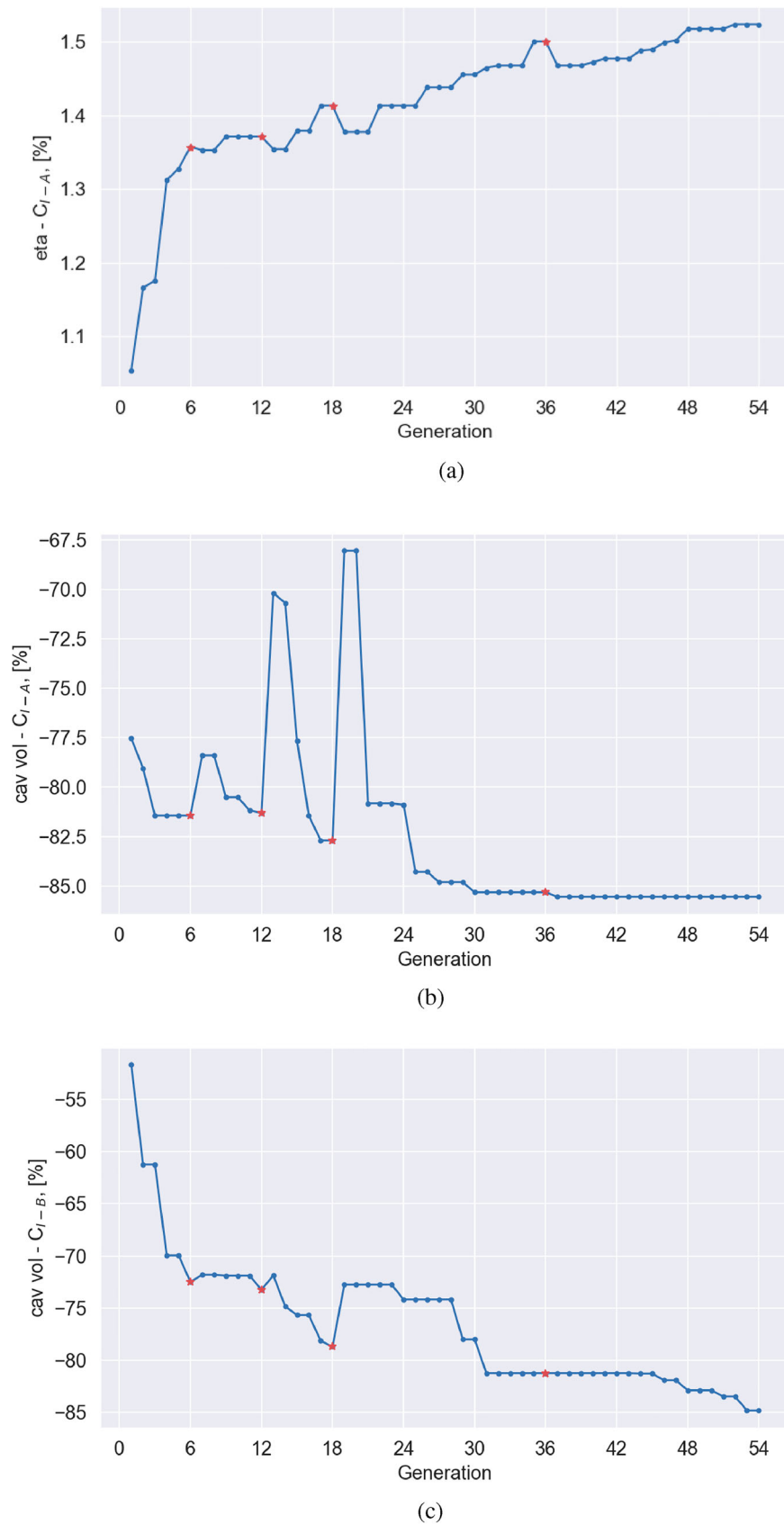
Figure 5. Convergence of the algorithm for the three objectives, percentage change to baseline – Design I. (a) efficiency C_{I-A} (b) cavity volume C_{I-A} (c) cavity volume C_{I-B} (This figure is available in colour online).
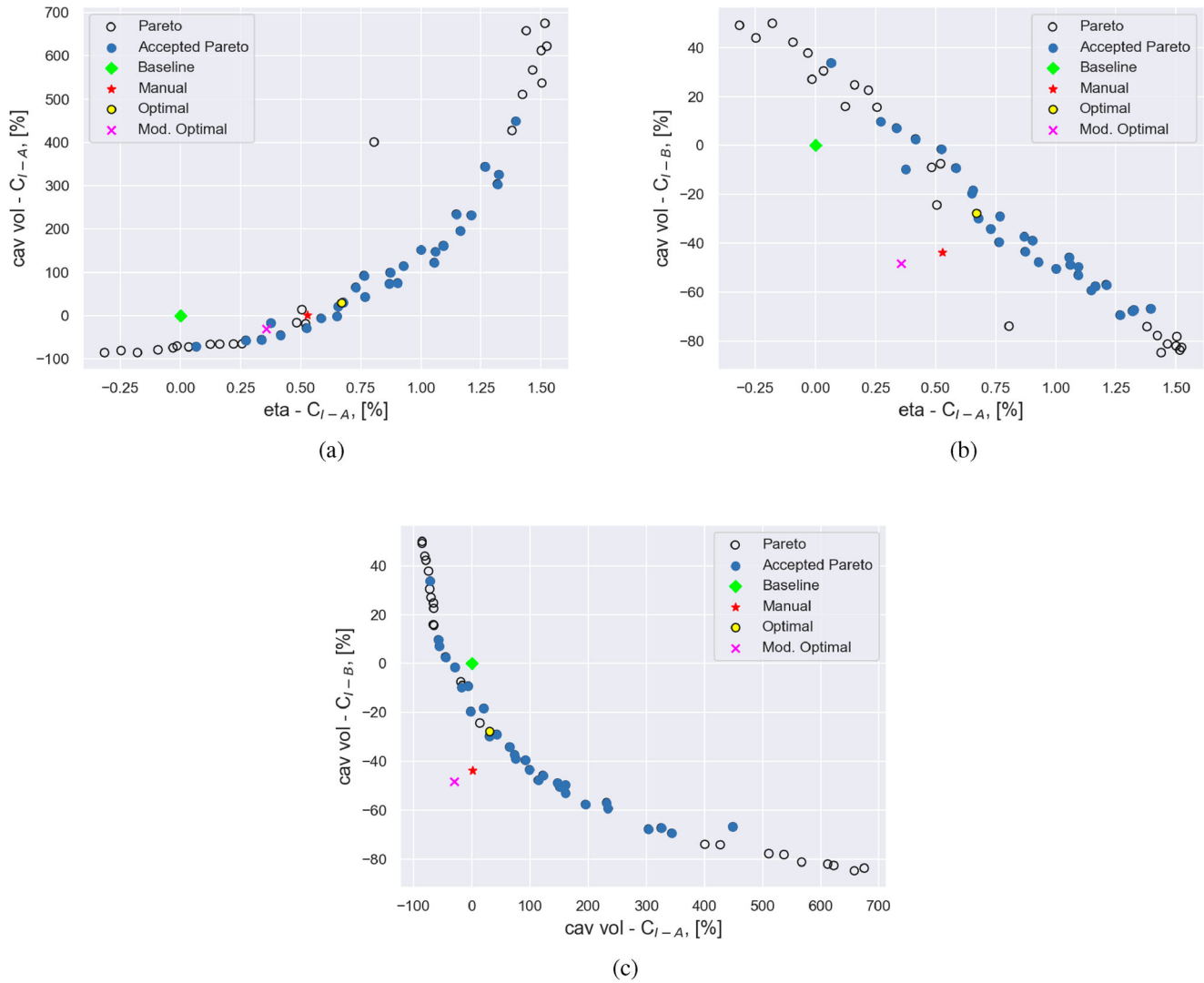
(a)

(b)

(c)

Figure 6. Final Pareto frontier including: manual, baseline, optimal & mod. optimal designs, percentage change to baseline – Design I. (a) efficiency C_{I-A} – cavity volume C_{I-I} (b) efficiency C_{I-A} – cavity volume C_{I-B} (c) cavity volume C_{I-A} – cavity volume C_{I-B} (This figure is available in colour online).

- Leading edge: Radius increase by 0.5 mm and HM curve increase at 0.3 –0.5R to increase the angle of attack tolerance
- Chord length curve: Increase at 0.6 –0.8R to reduce the suction side sheet cavitation.
- Skew: Increase angle by 1 degree to reduce pressure pulses.

From the designer's modifications, it is evident that the chord length could have been added as a design variable of the optimisation problem, and maybe even better solutions could have been obtained.

The manually improved optimal design or modified optimal design is presented in Figure 6 with the 'x' marker. The percentage change of the performance of the objectives for th optimal and the modified optimal designs compared to the manual design is shown in Table 5. The optimal design has better performance in efficiency

(0.14%), but higher cavity volume in C_{I-A} (29%) and in C_{I-B} (28.6%). After the modifications of the designer, the modified optimal design has a decreased efficiency compared to the manual design by 0.17%, while the cavity volume in C_{I-A} is improved by 31.2% compared to the manual design, and in C_{I-B} by 7.8%.

4.1.4. Geometry

The curves of the design variables (P/D, FM, HM) for the baseline, manual, optimal and modified optimal Design I are presented in Figure 7. The values of the design variables have been hidden in the plots for protection of commercial interests of Kongsberg Maritime AB.

In Figures 7(a) and 7(b), the P/D and FM curves of the optimal design have approximately the same shape as the curves of the baseline. The manual modifications on the P/D curve by the blade designer are minor compared to the optimal design. The modifications of the FM curve of the modified optimal design when compared to the optimal design are more evident, with decreased values from the root until the midchord of the blade and increased values from the midchord until almost the tip. In Figure 7(c), the HM curves are presented. No leading edge modification had been applied on the baseline design, therefore it has zero values. The
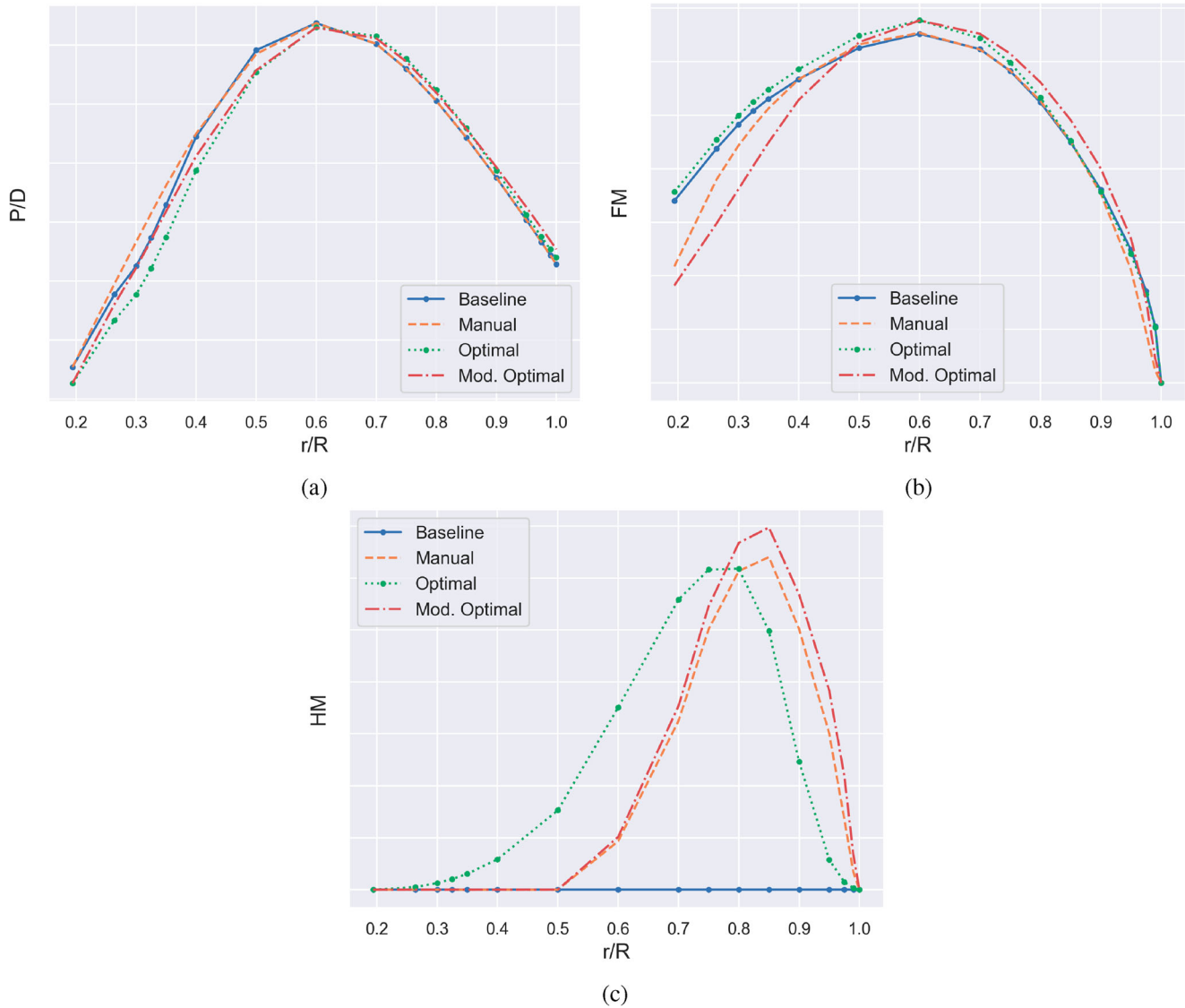
Table 5. Percentage change in performance of optimal and modified optimal designs compared to manual – Design I.

Objective	Optimal design [%]	Mod. optimal design [%]
max η_{I-A}	0.14	−0.17
min cav-vol$_{I-A}$	29.0	−31.2
min cav-vol$_{I-B}$	28.6	−7.8

Figure 7. Design variable curves for P/D, FM, HM including the designs: manual, baseline, optimal & modified optimal – Design I. (a) P/D (b) FM (c) HM (This figure is available in colour online).

resulting HM curve shape of the optimal design has been modified a lot by the blade designer, since at 0-0.5R the HM is zero and eventually the curve came to be very similar as the curve of the manual design.

The modifications that have been performed by the blade designer, especially in the P/D and FM curves, were required in

Figure 8. Cavity shape for modified optimal design with SS (left) and PS (right) cavitation – Design I (This figure is available in colour online).

the specific project after the optimisation in order to obtain a representative and realisable geometry. Also, the major modifications done for the HM curve, could have been avoided with a better set-up prior to the optimisation.

4.1.5. Cavitation
The cavity shape of the modified optimal design is shown in Figure 8. The size of the cavity shape of both conditions C_{I-A} and C_{I-B} is evidently smaller than the one of the manual design, which is presented in Figure 4(b).

4.2. Design II

4.2.1. Convergence
The convergence of the algorithm for the four objectives is presented in Figure 9 and the results are presented as a percentage change to the baseline design. Similarly as with Design I, the performance of the objectives of the designs worsens after the generations 6, 12 and 18, where manual cavitation evaluations were utilised. This drop of the performance is also observed with
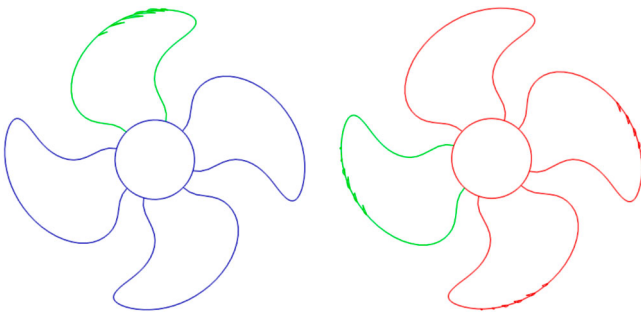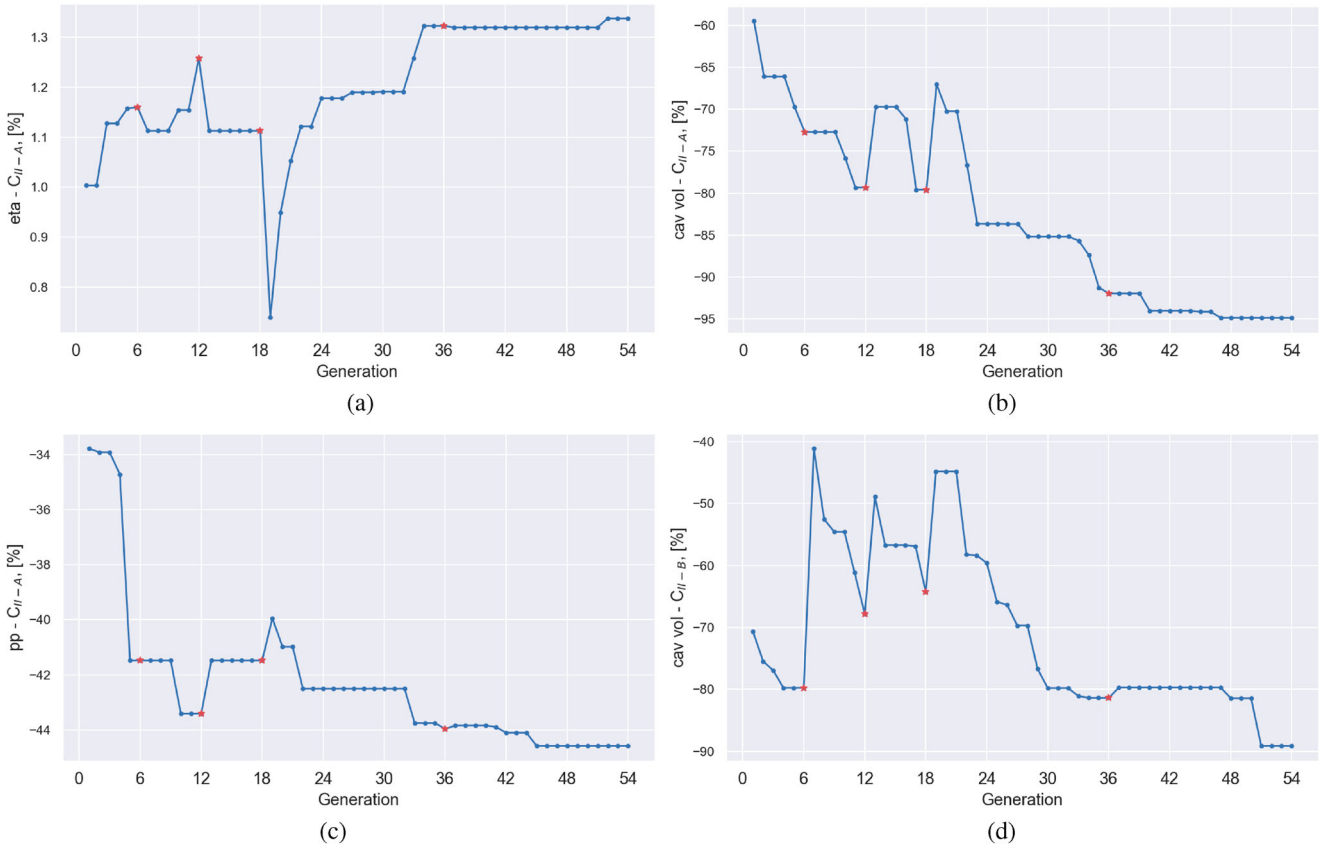
Figure 9. Convergence of the algorithm for the four objectives, percentage change to the baseline – Design II. (a) efficiency C_{II-A} (b) cavity volume C_{II-A} (c) pressure pulses C_{II-A} (d) cavity volume C_{II-B} (This figure is available in colour online).

the use of the MLP in generation 36, but the impact is less significant.

4.2.2. Pareto plots

The Pareto frontiers for the performance of the four objectives are presented in six Pareto plots in Figure 10, with the objectives combined two by two. The results are presented as a percentage change to the baseline design. The designer during the cavitation evaluation of the frontier has accepted 23 out of the 52 designs (44%). By comparing the manual design to the accepted Pareto designs, there are several designs that can be considered better than the manual design.

4.2.3. Optimal design & manual modifications

The blade designer selected one design (point with yellow circle 'o' in Figure 10), which has better performance than the manual design in the efficiency, the cavity volume of condition C_{II-B} and the pressure pulses are almost the same. It is first checked whether the design has a geometry that can be considered deliverable for manufacturing without any manual modifications, and only minor modifications are needed to achieve a production ready blade. By comparing the two designs, the main geometrical differences are that the optimal design has lower blade area ratio (EAR) compared to the manual design, something that led to higher efficiency. The camber at the tip of the optimal design is higher than the manual design, which offered lower cavity volume in condition C_{II-A}, but the lower values in the curve of the leading edge modification led to increased cavity volume in C_{II-B}. The cavity volume in condition C_{II-B} is actually quite high, but the advantage of the higher efficiency prevails. Finally, the chord length distribution

was a bit flat at 0.7R, and the designer preferred a smoother geometry at that point. Therefore, the designer aimed at doing some minor manual modifications in the camber, chord length and leading edge modification curves, while maintaining the efficiency constant. The modifications are the following:

- Pitch curve: Local increase at the tip of the blade.
- Camber curve: Decrease at the tip and the root in order to compensate the increase of the pitch.
- Leading edge modification curve: Increase at the root, due to some small indication of root cavitation on the PS.
- Chord length curve: Increase at 0.7R for creating a more smooth curve.

The modified optimal design is presented in Figure 10 with the 'x' marker. The differences between the optimal and the modified optimal designs are very small, and the modified optimal design has slightly worse performance in the three objectives, but it maintains the same efficiency as the optimal design. However, the geometry of the modified optimal design after the manual modifications is considered acceptable to be manufactured. The percentage change of the performance of the objectives for the optimal and modified optimal designs compared to the manual design is shown in Table 6.

4.2.4. Geometry

The curves of the design variables (P/D, FM, HM, L and SK) for the baseline, manual, optimal and modified optimal designs are presented in Figure 11. The values of the design variables presented
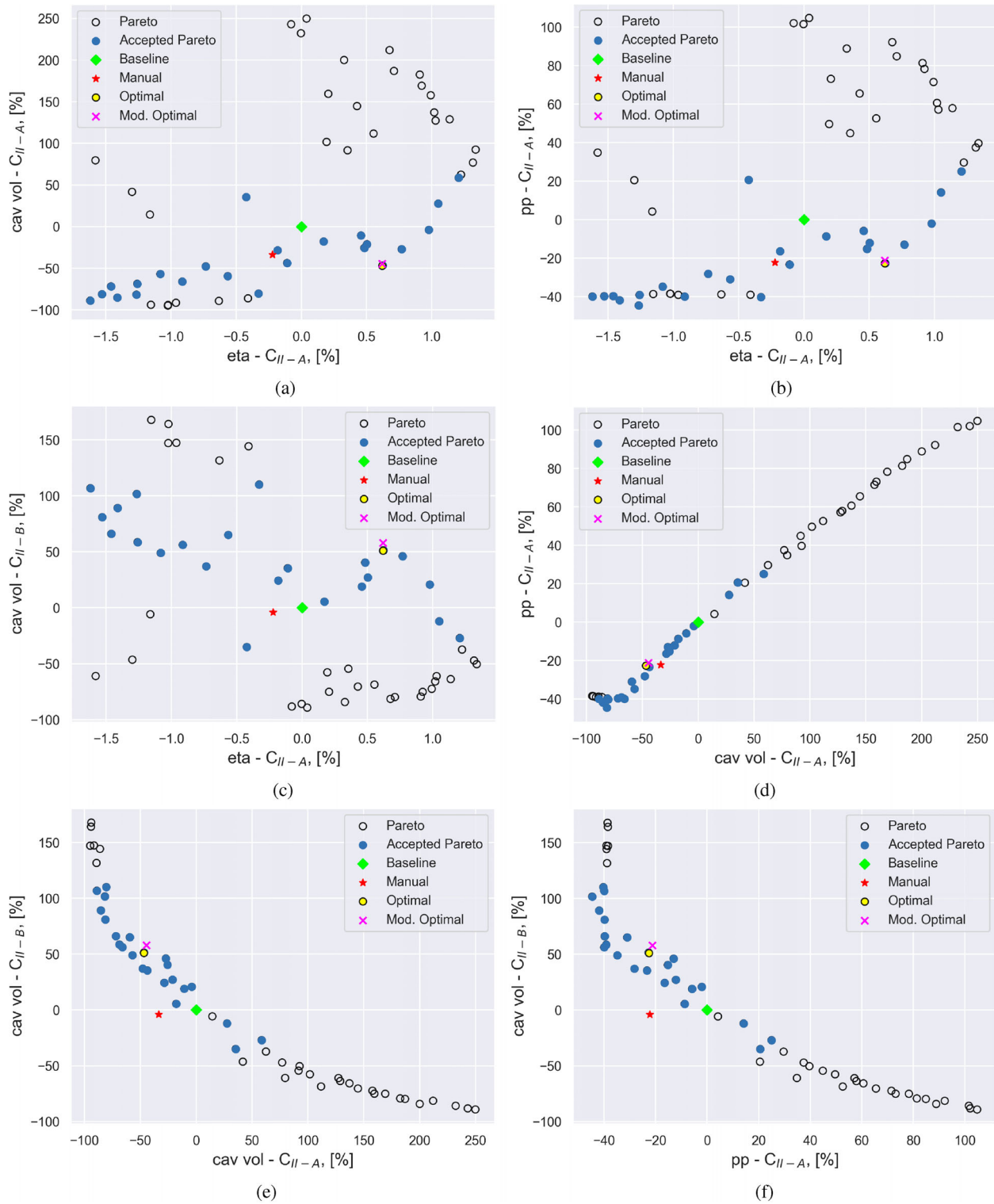
Figure 10. Final Pareto frontier including: manual, baseline, optimal & mod. optimal designs, percentage change to baseline-Design II. (a) efficiency C_{II-A} – cavity volume C_{II-I} (b) efficiency C_{II-A} – pressure pulses C_{II-A} (c) efficiency C_{II-A} – cavity volume C_{II-B} (d) cavity volume C_{II-A} – pressure pulses C_{II-A} (e) cavity volume C_{II-A} – cavity volume C_{II-B} (f) pressure pulses C_{II-A} – cavity volume C_{II-B} (This figure is available in colour online).

in the plots have been hidden for protection of commercial interests of Kongsberg Maritime AB.

The shape of the P/D curves in plot 11(a) of all designs are quite similar. The values of the modified optimal design at the root until the midchord are increased, and from the midchord until the tip are decreased, compared to the values of the optimal design. In

Table 6. Percentage change in performance of optimal and modified optimal designs compared to manual – Design II.
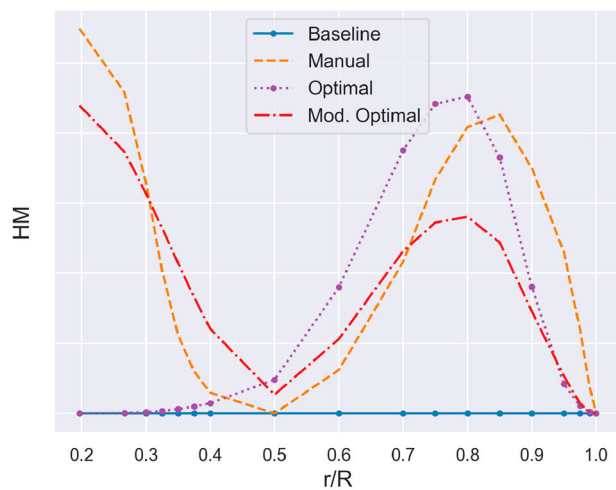
Objective	Optimal Design [%]	Mod. Optimal Design [%]
max η_{II-A}	0.83	0.83
min pp_{II-A}	0.4	1.3
min cav-vol$_{II-A}$	−17.5	−16.8
min cav-vol$_{II-B}$	58.0	64.5
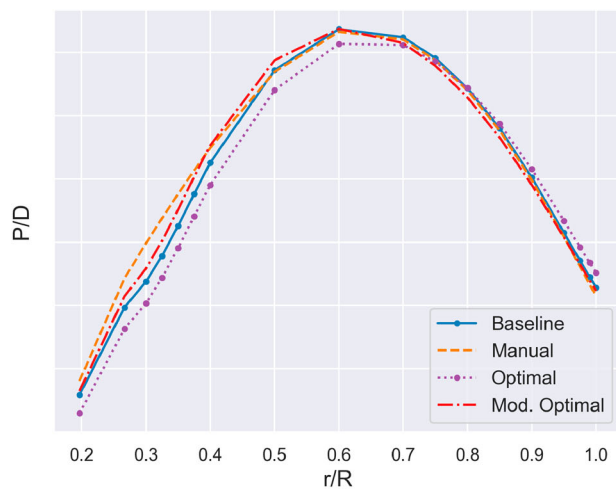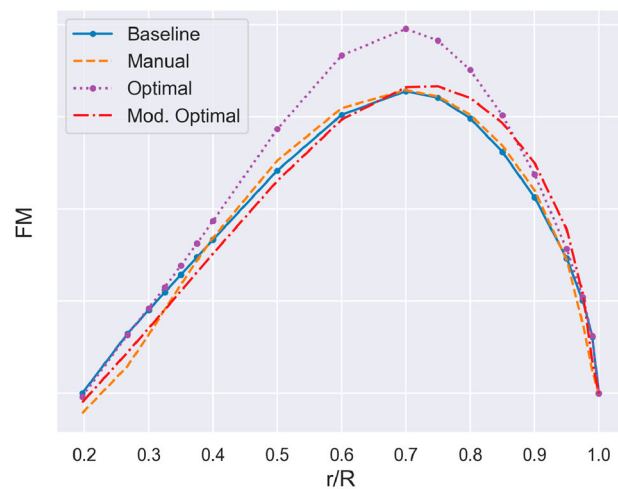
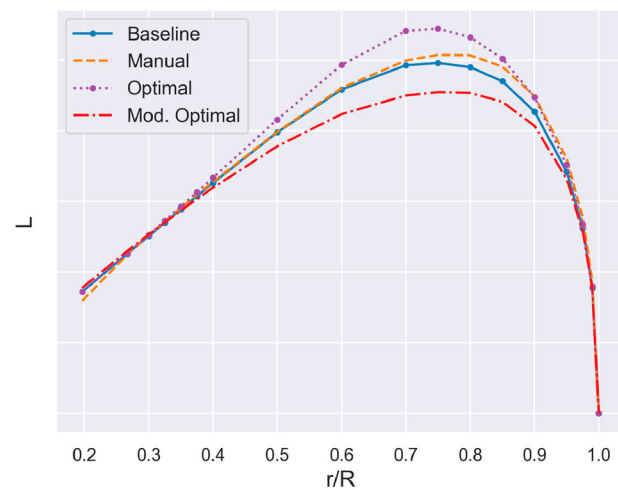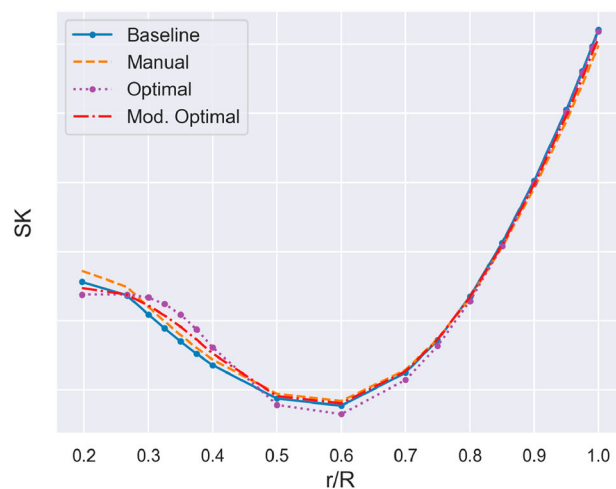**Figure 11.** Design variable curves for P/D, FM, HM, L, SK including the designs: manual, baseline, optimal & modified optimal – Design II. (a) P/D (b) FM (c) HM (d) L (e) SK (This figure is available in colour online).
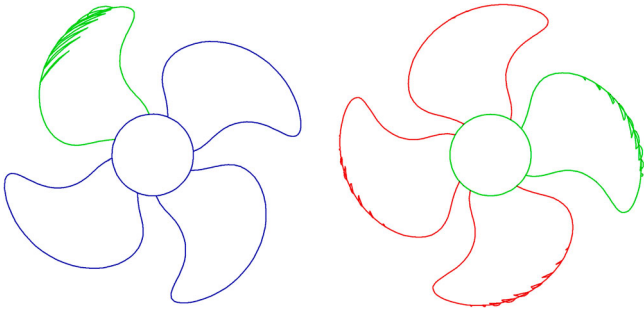
Figure 12. Cavity shape for modified optimal design with SS (left) and PS (right) cavitation – Design II (This figure is available in colour online).

addition to this, the optimal design follows the shape of the baseline design. The shape of the FM curve in plot 11(b) of the optimal design at 0.5 –0.8R is increased compared to all other designs. The HM curve is presented in plot 11(c) and similarly as for Design I, no leading edge modification had been applied on the baseline design. The result of the optimisation for the optimal design is a bell-shaped curve. However, the designer has modified the HM curve both for the manual and the modified optimal designs, by increasing the HM value at the blade root, decreasing at the midchord and from the midchord until the blade tip, there is a bell-shaped curve. The L curves are presented in 11(d), and all designs have approximately the same shape. The optimal design has more increased values at 0.45 –0.9R compared to the manual and modified optimal designs. Finally, the SK curves, presented in plot 11(e), have almost the same shape and values in all designs.

Similarly as for Design I, the manual modifications performed by the blade designer on the P/D, FM, L and SK curves were required in the specific project so that a realistic geometry is finally obtained. The major modifications done for the HM curve could have been avoided with a better set-up prior to the optimisation.

4.2.5. Cavitation
The cavity shape of the modified optimal design is shown in Figure 12. The size of the PS cavity shape of condition C_{II-B} is much higher than the one of the manual design, but the advantage of higher efficiency was deemed more important according to the designers for the specific scenario, especially as the level of pressure pulses could be kept constant.

4.3. Machine learning results

The ML results for both designs are presented in this section. The MLP was utilised after the third optimisation run and the best ML model in each case was used for the cavitation evaluation prediction of the entire population of the fourth run. The best ML algorithm of Design I is the NN, which offered a prediction accuracy of 79.5% with the following hyperparameters:

- activation function for the hidden layer = tanh
- alpha = 0.05
- hidden layer sizes = (50, 100, 50)
- learning rate = constant
- maximum iterations = 100
- solver = adam (stochastic gradient-based optimiser)

The best ML algorithm for Design II is the SVM, which offered an accuracy equal to 72.8%, with the following hyperparameters:

- C = 100
- gamma = 0.01
- kernel = radial basis function

By comparing the results of the prediction accuracy of the studies in Gypa et al. (2021), Gypa et al. (2022) to the present study, the accuracy has dropped. However, the prediction accuracy of the model cannot be better than the manual evaluations that it has been trained on, since it only reflects the performance of the manual evaluation. In more detail, in this scenario SS and PS cavitation are evaluated for the same scenario. The designer judges the cavitation characteristics of each design by looking at both types of cavitation. This means that the decision on whether a design is accepted or not becomes harder and for some similar designs that the cavitation differences are very small, the blade designer might evaluate them inconsistently. Since the manual evaluations are utilised as input to the ML models, this input can be inconsistent as well. Thus, it is reasonable that the prediction accuracy decreased.

ML is used as part of the optimisation process, with the expectation to accelerate the efficiency of the design process. With a prediction accuracy of 70–80%, some designs will pass to the first generation of the next optimisation run as accepted even though they were actually not. However, the NSGA-II still promotes designs with the highest performance to the following generations. Therefore even with lower predictability, ML is a useful tool for the optimisation, because the designers will not manually evaluate the cavitation of the designs of an entire run.

Apart from the prediction accuracy of an ML model, understanding and explaining the output of the model is important as well. This can be done with the aid of SHAP (SHapley Additive exPlanations) values (Lundberg and Lee 2017). The goal of SHAP values is to explain the prediction by computing the contribution of each feature to the prediction. In Figure 13, the variable importance plots for Designs I and II are shown. Variable importance plots show which variables contribute most to the predictive power of the model. The x-axis presents the average of the absolute SHAP values per feature and the y-axis presents the features in descending order of importance. In Figure 13(a), the P/D at 1.0R is the most important feature, while the HM at 0.8R and FM at 0.19R are the least important features. Similar results are obtained from Figure 13(b), where again the P/D at 1.0R is the most important feature, followed by the L at 0.8R and FM at 0.7R. The P/D at 0.2R and HM at 0.8R are the least important features for the prediction of the SVM.

5. Concluding remarks

A methodology is proposed in this study for solving constrained, multi-objective blade design optimisation problems efficiently, as an everyday task of industrial applications. The methodology combines interactive optimisation with machine learning. The blade designer evaluates cavitation characteristics as part of the optimisation systematically and this information is used for guiding the algorithm towards solutions with the desirable cavitation characteristics and for training machine learning models that are later used for prediction of cavitation evaluation.

The case studies consider two advanced propeller designs of twin CPPs for ROPAX vessels. Both scenarios were complex, representing real commercial design tasks involving several design variables, objectives and constraints and with conditions that have either suction side or pressure side cavitation. The challenge has been to find optimal solutions that will fulfil the objectives and
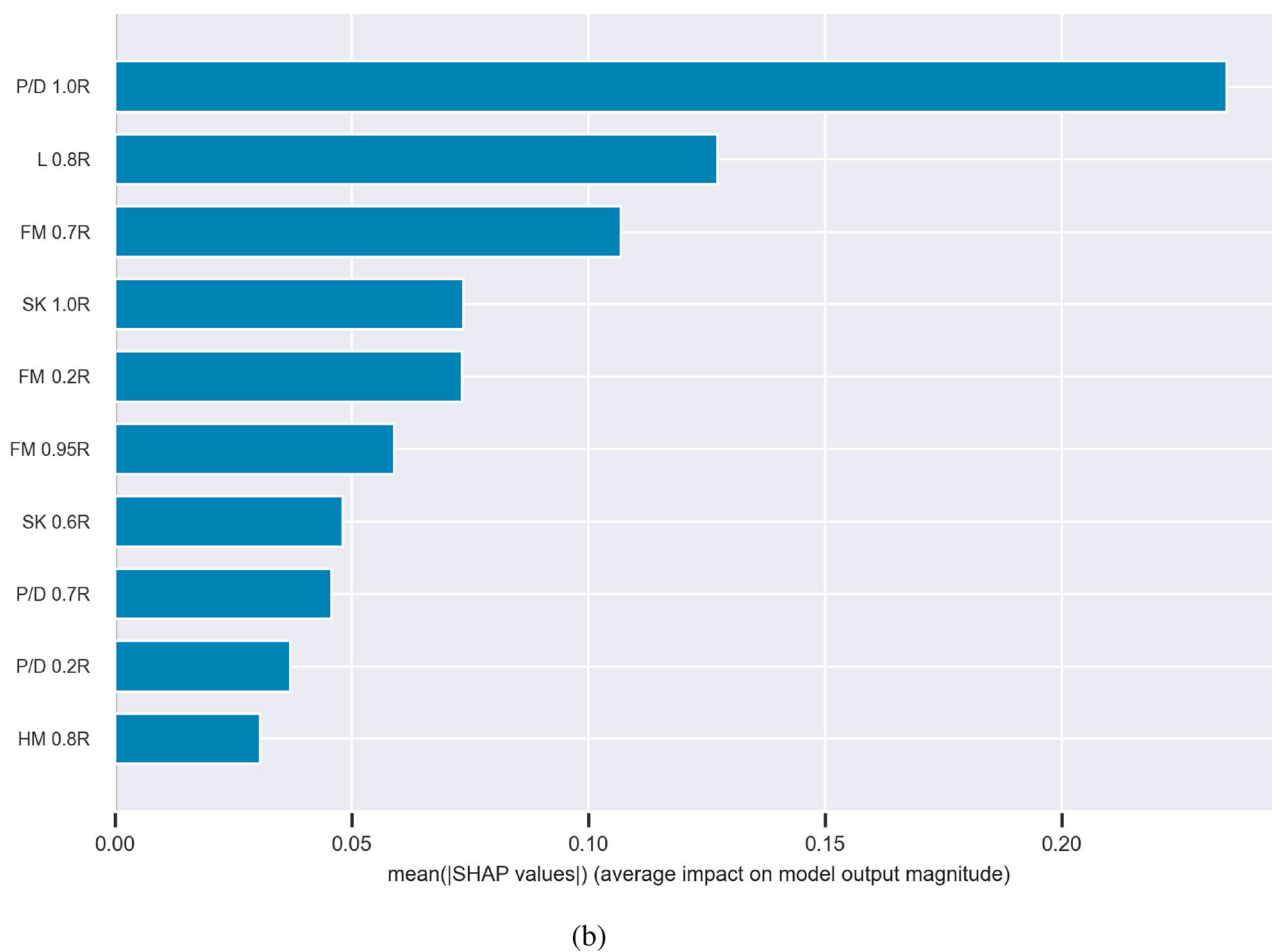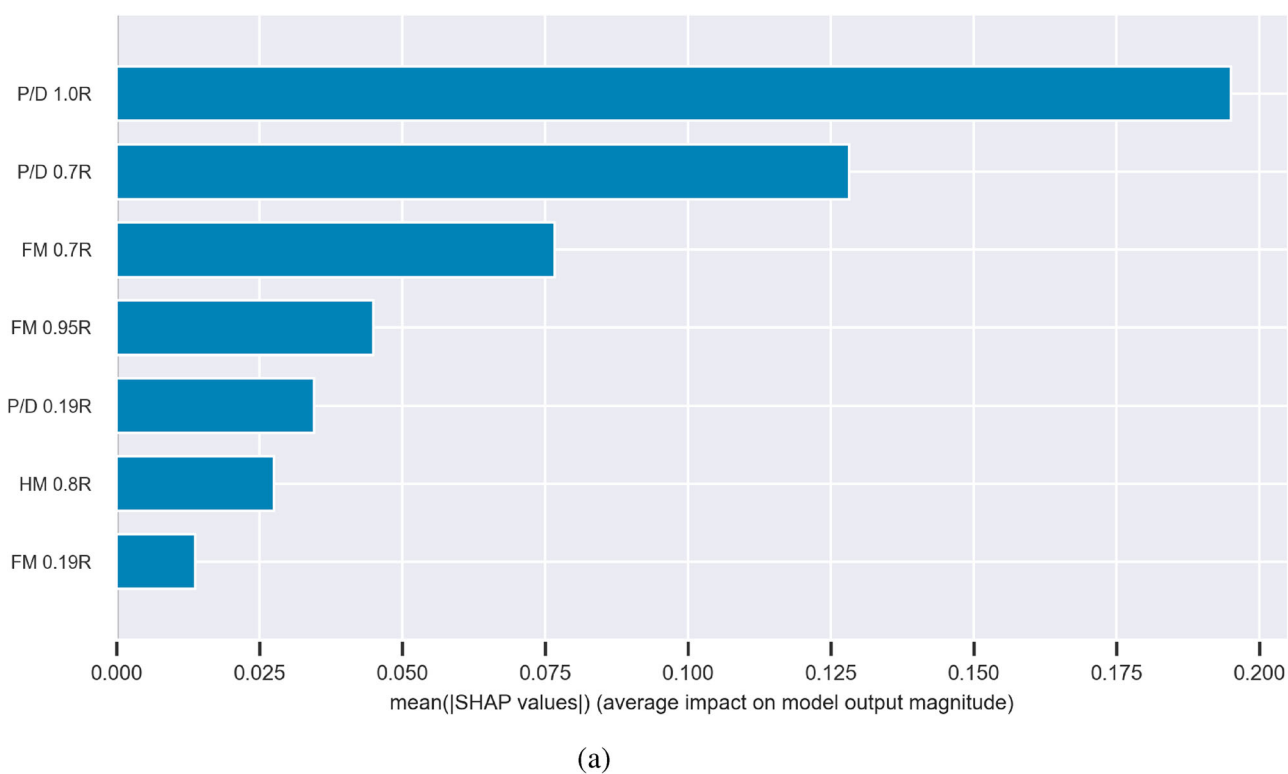
Figure 13. SHAP values: variable importance plots. (a) Design I (b) Design II (This figure is available in colour online).

quantitative constraints, and in parallel have satisfactory cavitation characteristics.

The obtained designs were compared to the delivered manual designs by the blade designer. The results of both case studies showed that the optimisation procedure led to higher performance. Both Pareto frontiers included several designs that were better compared to the manual designs, in terms of performance and cavitation characteristics. Minor manual modifications were performed by the blade designer, in order to obtain ready-to-be-manufactured geometries.

Using ML proved to be a useful support tool of the optimisation, which accelerated the process, since the designers did not evaluate the optimisation runs with larger populations of individuals. For the input of the ML, there were some designs that it was harder for the designer to decide whether they should be accepted or not, because for example they had satisfactory SS cavitation, but the PS cavitation was on the limit. This led to inconsistent evaluations for some designs, something that should be investigated further.

The proposed methodology found to be a good support tool of the entire optimisation process, according to the results and the blade designers. However, in order to better understand the further needs for the specific tool, more information is needed by the designers after utilising it for their everyday design tasks. A human factor research with the participation of blade designers could aid towards that direction. There are several questions that need to be answered, such as after how many user evaluations do the blade designers feel fatigued, if they should be enabled to alternate the geometry of the designs during the optimisation and for which design scenarios should the MLP be used. This process could also create ideas on more new interactive steps that could lead to faster convergence and to more efficient solutions. Also, through a human factor study, it would be possible to quantify the cost benefit of using the proposed methodology, compared to a solely manual process.

Acknowledgements

Disclosure statement

No potential conflict of interest was reported by the author(s).

References

Berger S, Druckenbrod M, Pergande M, Abdel-Maksoud M. 2014. A two-stage optimisation method for full-scale marine propellers working behind a ship. Ship Technol Res. 61(2):64–79. doi: 10.1179/str.2014.61.2.001

Chen T, Guestrin C. 2016. Xgboost: a scalable tree boosting system. In: Proceedings of the 22nd ACM SIGKDD international conference on knowledge discovery and data mining, p. 785–794.

Deb K, Pratap A, Agarwal S, Meyarivan T. 2002. A fast and elitist multiobjective genetic algorithm: Nsga-ii. IEEE Trans Evol Comput. 6(2):182–197. doi: 10.1109/4235.996017

Doijode PS, Hickel S, Van Terwisga T, Visser K. 2022a. A machine learning approach for propeller design and optimization: Part i. Appl Ocean Res. 124:103178. doi: 10.1016/j.apor.2022.103178

Doijode PS, Hickel S, Van Terwisga T, Visser K. 2022b. A machine learning approach for propeller design and optimization: Part ii. Appl Ocean Res. 124:103174. doi: 10.1016/j.apor.2022.103174

Fix E, Hodges JL. 1989. Discriminatory analysis nonparametric discrimination: consistency properties. Int Stat Rev/Revue Int De Statist. 57(3):238–247. doi: 10.2307/1403797

Foeth EJ, Lafeber F. 2015. Systematic propeller optimization using an unsteady boundary element method. In: Fourth International Symposium on Marine Propulsors (SMP15); Austin, TX, USA.

Fuhs D. 2005. Evaluation of propeller unsteady force codes for noncavitating conditions. Technical Report. Naval Surface Warfare Center Carderock Division.

Gaggero S, Tani G, Villa D, Viviani M, Ausonio P, Travi P, Bizzarri G, Serra F. 2017. Efficient and multi-objective cavitating propeller optimization: an application to a high-speed craft. Appl Ocean Res. 64:31–57. doi: 10.1016/j.apor.2017.01.018

Guan G, Zhang X, Wang P, Yang Q. 2022. Multi-objective optimization design method of marine propeller based on fluid-structure interaction. Ocean Eng. 252:111222. doi: 10.1016/j.oceaneng.2022.111222

Gypa I. 2021. Interactive optimisation in marine propeller design. Licentiate Thesis.

Gypa I, Bensow R, Wolff K, Gustafsson R. 2020. Interactive evolutionary computation for propeller design optimization of wind-assisted vessels.

Gypa I, Jansson M, Bensow R. 2022. Cavitation nuisance identification through machine learning during propeller optimisation. In: Seventh International Symposium on Marine Propulsors, Wuxi, China.

Gypa I, Jansson M, Gustafsson R, Werner S, Bensow R. 2023. Controllable-pitch propeller design process for a wind-powered car-carrier optimising for total energy consumption. Ocean Eng. 269:113426. doi: 10.1016/j.oceaneng.2022.113426

Gypa I, Jansson M, Wolff K, Bensow R. 2021. Propeller optimization by interactive genetic algorithms and machine learning. Ship Technol Res. 70(1):56–71. doi: 10.1080/09377255.2021.1973264

He L. 2010. Numerical simulation of unsteady rotor/stator interaction and application to propeller/rudder combination [dissertation].

He L, Chang S, Kinnas S. 2010. MPUF-3A Version 3.0. Technical Report. University of Texas.

Hopfield JJ. 1982. Neural networks and physical systems with emergent collective computational abilities. Proc Natl Acad Sci. 79(8):2554–2558. doi: 10.1073/pnas.79.8.2554

Huisman J, Foeth EJ. 2017. Automated multi-objective optimization of ship propellers. In: Fifth International Symposium on Marine Propulsors SMP'17, Espoo, Finland.

Karimi R, Shokri V, Khishe M, Jameie M. 2022. Marine propeller design using evolving chaotic autonomous particle swarm optimization. Wirel Pers Commun. 125(2):1653–1675. doi: 10.1007/s11277-022-09625-x

Kerwin J, Kinnas S, Wilson MB. 1986. Experimental and analytical techniques for the study of unsteady propeller sheet cavitation. In: Symposium on Naval Hydrodynamics, 16th, Berkeley, California.

Kinnas S, Lee H, Young YL. 2003. Modeling of unsteady sheet cavitation on marine propeller blades. Int J Rotating Mach. 9(4):263–277. doi: 10.1155/S1023621X03000241

Kongsberg hydrodynamic design team. 2020. Private communication.

Lee CS. 1979. Prediction of steady and unsteady performance of marine propellers with or without cavitation by numerical lifting-surface theory [dissertation]. Massachusetts Institute of Technology.

Lundberg SM, Lee SI. 2017. A unified approach to interpreting model predictions. Adv Neural Inf Process Syst. 30.

Moulijn J. 2015. Application of various computational methods to predict the performance and cavitation of ducted propellers. In: Fourth International Symposium on Marine Propulsors smp.

Pedregosa F, Varoquaux G, Gramfort A, Michel V, Thirion B, Grisel O, Blondel M, Prettenhofer P, Weiss R, Dubourg V, Vanderplas J, Passos A, Cournapeau D, Brucher M, Perrot M, Duchesnay E. 2011. Scikit-learn: machine learning in python. J Mach Learn Res. 12:2825–2830.

Quinlan JR. 1986. Induction of decision trees. Mach Learn. 1:81–106.

Tadros M, Ventura M, Soares CG. 2022. Optimization procedures for a twin controllable pitch propeller of a ropax ship at minimum fuel consumption. J Mar Eng Technol. 0:1–9.

Törnros S, Klerebrant O, Korkmaz E, Huuva T. 2019. Propeller optimization for a single screw ship using bem supported by cavitating cfd. In: Proceedings of the Sixth International Symposium on Marine Propulsors SMP.

Valdenazzi F, Conti F, Gaggero S, Grassi D, Vaccaro C, Villa D. 2019. A practical tool for the hydro-acoustic optimization of naval propellers. In: Proceedings of the 8th Conference on Computational Methods in Marine Engineering (Marine 2019), Gothenburg, Sweden.

Vapnik VN. 1995. The nature of statistical learning theory. Berlin, Heidelberg: Springer-Verlag.

Vesting F. 2015. Marine propeller optimisation – strategy and algorithm development [dissertation]. Chalmers University of Technology.

Wahde M. 2008. Biologically inspired optimization methods: an introduction. WIT press.